J. Fluid Mech. (1987), *vol.* 174, *pp.* 357–379
Printed in Great Britain

Nonlinear transition in three-dimensional convection

By R. KESSLER†
Institute for Theoretical Fluid Mechanics, DFVLR, Bunsenstrasse 10,
D-3400 Göttingen, West Germany

(Received 1 May 1985 and in revised form 2 May 1986)

Steady and oscillatory convection in a rectangular box heated from below are studied by means of a numerical solution of the three-dimensional, time-dependent Boussinesq equations. The effect of the rigid sidewalls of the box on the spatial structure and the dynamical behaviour of the flow is analysed. Both conducting and adiabatic sidewalls are considered. Calculated streamlines illustrate the three-dimensional structure of the steady flow with Prandtl numbers 0.71 and 7. The onset and the frequency of the oscillatory instability are calculated and compared with available experimental and theoretical data. With increasing Rayleigh number a subharmonic bifurcation and the onset of a quasi-periodic flow can be observed. A comparison of the different time-dependent solutions shows some interesting relations between the spatial structure and the dynamical behaviour of the confined flow.

1. Introduction

Thermal convection in a fluid layer heated from below has been studied extensively. This flow exhibits a sequence of transitions from steady laminar to turbulent flow which allows fundamental studies of nonlinear hydrodynamics. In fluid layers of infinite horizontal extent the convection flow starts at the critical Rayleigh number Ra_c with steady two-dimensional rolls. The stability of this flow with respect to three-dimensional or time-dependent disturbances is well known and has been described in numerous theoretical and experimental papers (Busse 1981; Koschmieder 1981; Zierep & Oertel 1981).

In experiments the infinite fluid layer is approximated by a large-aspect-ratio container where sidewall effects can be neglected. However, considering low-aspect-ratio boxes, the influence of the side-walls cannot be neglected. The confined flow now also depends on the geometry of the box, as well as on the thermal properties of the sidewalls. Linear stability analysis and experiments show the stabilizing effect of the vertical boundaries on the onset of convection flow (Davis 1967; Stork & Müller 1972). The exact solution of the confined flow must be three dimensional even at the onset of convection, as was proved by Davies-Jones (1970) and Frick & Clever (1980). Therefore, a transition from two-dimensional to three-dimensional steady stages predicted and observed in infinitely extending fluid layers does not occur in low-aspect-ratio boxes. Benjamin (1978) also showed that the stability behaviour and the bifurcations of viscous flows can be changed considerably by introducing a finite geometry. Contrary to the possibility of a continuous variation of the wavenumber of the periodic flow in infinite layers, the wavelength of the convection

† Present address: Lehrstuhl für Strömungsmechanik, Universität Erlangen, Egerlandstrasse 13, D-8520 Erlangen, West Germany.

rolls in boxes can be changed only by a discrete variation of the number of rolls. In experiments using different convection boxes this nonlinear wavenumber-selection phenomenon was investigated during the transition from steady to oscillatory and finally to turbulent convection (Oertel 1980; Jäger 1982). In low-aspect-ratio boxes only a few solutions with different numbers of convection rolls exist. However, in experiments Gollub & Benson (1980) observed different flows having the same number of rolls. Although the differences between the flows are relatively small, each one of the configurations seems to be stable for a long time. This phenomenon is explained by the influence of the initial conditions on the experiments. This statement agrees with theoretical results of Benjamin (1978), who suggested stable solutions in viscous flows that can only be produced by special initial conditions.

The goal behind most of the experiments in small boxes is to study the transitions to various time-dependent flows, which occur with increasing Rayleigh number. Varying the Prandtl number, the geometry and the initial conditions, Gollub & Benson (1980) identified four distinct sequences of instabilities in the convection flow: two or three independent frequencies, phase-locking phenomena of these frequencies, intermittent non-periodic flow and period-doubling bifurcation of periodic flows. Subharmonics were also observed by Jäger (1982) in experiments with similar geometry. Libchaber & Maurer (1980) and Libchaber, Laroche & Fauve (1982) studied low-Prandtl-number fluids in various boxes with a magnetic field oriented parallel to the axis of the convection rolls. These experiments show a sequence of period-doubling bifurcations and agree well with theoretical predictions of Feigenbaum (1979).

Gollub, Benson & Steinman (1980) observed that rather small variations of the mean flow can produce major qualitative changes in the sequence of instabilities. Using laser-Doppler methods they obtained contour maps of both the time-averaged flow and the subharmonic amplitude in a horizontal section within the box, which give some information about the spatial structure of the time-dependent flow. General relations between the spatial structure of the flow and the dynamical behaviour of the system are still unknown.

In addition to experimental results, numerical simulations of the three-dimensional convective flow in small containers can give important information about the onset of various time-dependent instabilities. The data of the temperature and the velocity field obtained by a three-dimensional time-dependent solution can give detailed information about the spatial and temporal behaviour of the flow field. Recent numerical calculations of Upson *et al.* (1983) show an oscillatory convection flow in a box with adiabatic sidewalls. The calculated frequency agreed with the experimental results of Maurer & Libchaber (1979). Two frequencies with an equal amplitude appearing in the power spectrum were expounded as a reference to a subharmonic bifurcation. Another interpretation of this effect will be discussed.

In this paper steady and time-dependent calculations of the convection flow in a box with the aspect ratio length:width:height of 4:2:1 are presented. To avoid errors related to numerical dissipation a Galerkin method is used to solve the three-dimensional Boussinesq equations. First we will describe the three-dimensional effects in the steady convection flow to clarify the influence of conducting or adiabatic sidewalls. With increasing Rayleigh number the onset of the oscillatory instability is calculated for various Prandtl numbers. The critical Rayleigh numbers and the frequencies of the oscillations agree with corresponding experimental results. Power spectra of the temperature and the velocity components are compared, and their dependence on the position in the flow field is discussed. For certain parameters a

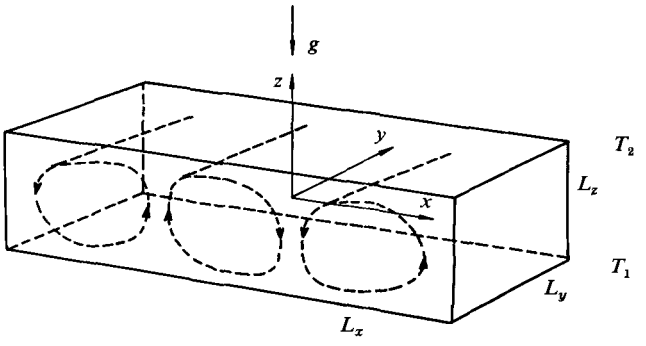

FIGURE 1. Principal sketch of the rectangular box and a possible three-roll structure.

subharmonic instability of the oscillatory flow and the onset of quasi-periodic flow is observed. A spectral analysis allows us to determine the spatial structure of the subharmonic frequency. An interesting relationship is found by comparison of the spatial structure of the mean flow with the distribution of the subharmonic amplitude.

The mathematical formulation of the problem and a brief description of our numerical technique is given in §2. In §3 the steady solutions are discussed by means of calculated streamlines. The results concerning the oscillatory convection and the onset of period-doubling bifurcation are presented in §4, and discussed in the light of other theoretical and experimental results in §5.

2. Mathematical formulation and numerical method

We consider a fluid layer in a horizontal rectangular box of height L_z and horizontal extents L_x and L_y (figure 1). The upper and the lower boundary are kept at the constant temperatures T_2 and T_1, respectively. Using the Boussinesq approximation we obtain dimensionless equations for the velocity vector $\boldsymbol{v} = (u, v, w)$ and for the deviation θ from the static temperature distribution in the following form

$$Pr^{-1}\left(\frac{\partial \boldsymbol{v}}{\partial t} + \boldsymbol{v}\cdot\nabla\boldsymbol{v}\right) = -\nabla p + \nabla^2\boldsymbol{v} + Ra\,\theta\boldsymbol{k}, \tag{2.1a}$$

$$\nabla\cdot\boldsymbol{v} = 0, \tag{2.1b}$$

$$\frac{\partial\theta}{\partial t} + \boldsymbol{v}\cdot\nabla\theta = \boldsymbol{v}\cdot\boldsymbol{k} + \nabla^2\theta, \tag{2.1c}$$

where p is the pressure and $\boldsymbol{k}$ is the unit vector in the z-direction. The height L_z of the fluid layer, the vertical thermal diffusion time L_z^2/κ and the temperature difference $(T_1 - T_2)$ have been used as scales for length, time and temperature respectively, where κ is the thermal diffusivity. The parameter Ra is the Rayleigh number and Pr the Prandtl number, defined as

$$Ra = \frac{\gamma g (T_1 - T_2) L_z^3}{\kappa\nu}, \quad Pr = \frac{\nu}{\kappa},$$

where γ is the coefficient of thermal expansion, g is the acceleration due to gravity and ν is the kinematic viscosity. At all walls of the box the no-slip boundary condition is prescribed. At the horizontal boundaries the deviation θ of the temperature must vanish. The sidewalls are chosen to be either conducting or adiabatic, so the temperature deviation θ or its gradient normal to the wall is set equal to zero.

A Galerkin method is developed to solve (2.1). The advantage of this method is based on the analytical representation of the solution by series expansions. All spatial differentiations can be done analytically and numerical dissipation, as it appears in finite difference schemes, is avoided completely. In addition, the basis functions can be chosen such as to exactly satisfy all boundary conditions. By using non-divergent basis functions for the expansion of the velocity field, the pressure term can be eliminated. A general representation of a three-dimensional, non-divergent vector field is the following superposition

$$\boldsymbol{v} = \boldsymbol{\nabla} \times (\boldsymbol{\nabla} \times \boldsymbol{k}\phi) + \boldsymbol{\nabla} \times \boldsymbol{k}\psi, \tag{2.2}$$

where $\boldsymbol{k}$ is the unit vector in z-direction. By defining two new scalar functions $\psi^{(1)}$ and $\psi^{(2)}$ according to (2.3a), we can derive a formulation for a non-divergent vector field, which is equivalent to the general representation (2.2) and consists of two similar terms (2.3b):

$$\left.\begin{aligned} \partial_z \psi^{(1)} &= \partial_y \partial_z \phi - \partial_x \psi, \\ \partial_z \psi^{(2)} &= -\partial_x \partial_z \phi - \partial_y \psi, \end{aligned}\right\} \tag{2.3a}$$

$$\boldsymbol{v} = \boldsymbol{\nabla} \times \boldsymbol{i}\psi^{(1)} + \boldsymbol{\nabla} \times \boldsymbol{j}\psi^{(2)}, \tag{2.3b}$$

where $\boldsymbol{i}$ and $\boldsymbol{j}$ are unit vectors in the x- and y-direction, respectively. When the formulation (2.3b) is used to describe the velocity field, the no-slip condition causes a coupling of the two scalar functions $\psi^{(1)}$ and $\psi^{(2)}$

$$u = -\partial_z \psi^{(2)} = 0, \tag{2.4a}$$

$$v = \partial_z \psi^{(1)} = 0, \tag{2.4b}$$

$$w = \partial_x \psi^{(2)} - \partial_y \psi^{(1)} = 0. \tag{2.4c}$$

To avoid this coupling at the boundary of the integration domain, we extend (2.3b) by two additional scalar functions $\psi^{(31)}$ and $\psi^{(32)}$, which are chosen in such a way that they satisfy the condition (2.4c) in the whole integration region:

$$\boldsymbol{v} = \boldsymbol{\nabla} \times \boldsymbol{i}\psi^{(1)} + \boldsymbol{\nabla} \times \boldsymbol{j}\psi^{(2)} + \boldsymbol{\nabla} \times \boldsymbol{i}\psi^{(31)} + \boldsymbol{\nabla} \times \boldsymbol{j}\psi^{(32)}, \tag{2.5a}$$

with

$$\partial_x \psi^{(32)} - \partial_y \psi^{(31)} = 0. \tag{2.5b}$$

The extended formulation (2.5a) now makes it possible to use the simple boundary conditions (2.6) for the scalar fields $\psi^{(1)}$, $\psi^{(2)}$, $\psi^{(31)}$ and $\psi^{(32)}$ without any restriction on the generality of the representation of the vector field.

$$\partial_z \psi^{(1)} = \partial_z \psi^{(2)} = \partial_x \psi^{(2)} = \partial_y \psi^{(1)} = \partial_z \psi^{(31)} = \partial_z \psi^{(32)} = 0. \tag{2.6}$$

Now the only coupling between the scalar functions is given in the interior of the computational region by the governing equations (2.1), which essentially simplifies the numerical procedure.

The scalar functions $\psi^{(1)}$, $\psi^{(2)}$, $\psi^{(31)}$ and $\psi^{(32)}$ are expanded in terms of systems of orthogonal functions:

$$\psi^{(1)} = \sum_{i \leqslant L} \sum_{j \leqslant M} \sum_{k \leqslant N} a_{ijk}(t) \sin\left(i\pi\left(\frac{x}{l_x} + \frac{1}{2}\right)\right) C_j\left(\frac{y}{l_y}\right) C_k(z), \tag{2.7a}$$

$$\psi^{(2)} = \sum_{i \leqslant L} \sum_{j \leqslant M} \sum_{k \leqslant N} b_{ijk}(t) C_i\left(\frac{x}{l_x}\right) \sin\left(j\pi\left(\frac{y}{l_y} + \frac{1}{2}\right)\right) C_k(z), \tag{2.7b}$$

$$\psi^{(31)} = \sum_{i\leqslant L}\sum_{j\leqslant M}\sum_{k\leqslant N} c_{ijk}(t)\,\partial_x C_i\left(\frac{x}{l_x}\right) C_j\left(\frac{y}{l_y}\right)\cos\left(k\pi\,(z+\tfrac{1}{2})\right), \tag{2.7c}$$

$$\psi^{(32)} = \sum_{i\leqslant L}\sum_{j\leqslant M}\sum_{k\leqslant N} c_{ijk}(t)\,C_i\left(\frac{x}{l_x}\right)\partial y\, C_j\left(\frac{y}{l_y}\right)\cos\left(k\pi(z+\tfrac{1}{2})\right), \tag{2.7d}$$

with the dimensionless horizontal extends $l_x = L_x/L_z$ and $l_y = L_y/L_z$ of the box. The functions C_ν are the so-called 'beam-functions' documented by Harris & Reid (1958). They consist of even functions for odd ν and odd functions for even ν. By comparing the four expansions (2.7), a linear dependence can be found for the functions of the series (2.7*c*, *d*) with $k > 1$. Therefore, we can omit these functions without a loss of generality of the whole expansion. The temperature θ is represented by the expansions (2.8*a*) or (2.8*b*), assuming either conducting or adiabatic sidewalls.

$$\theta = \sum_{i\leqslant L}\sum_{j\leqslant M}\sum_{k\leqslant N} d_{ijk}\sin\left(i\pi\left(\frac{x}{l_x}+\frac{1}{2}\right)\right)\sin\left(j\pi\left(\frac{y}{l_y}+\frac{1}{2}\right)\right)\sin\left(k\pi(z+\tfrac{1}{2})\right), \tag{2.8a}$$

$$\theta = \sum_{i\leqslant L}\sum_{j\leqslant M}\sum_{k\leqslant N} d_{ijk}\cos\left((i-1)\,\pi\left(\frac{x}{l_x}+\frac{1}{2}\right)\right)\cos\left((j-1)\,\pi\left(\frac{y}{l_y}+\frac{1}{2}\right)\right)\sin\left(k\pi(z+\tfrac{1}{2})\right). \tag{2.8b}$$

The trigonometric functions as well as the beam-functions ensure a homogeneous resolution in the whole computational region. However, for some particular cases a high resolution near the wall is required for the accurate calculation of boundary layers. This can be achieved by using two sets of orthogonal polynomials, which satisfy the same boundary conditions as the trigonometric and beam-functions respectively. They can be constructed as a linear composition of the well-known Chebyshev polynomials $\tilde{T}_\mu$ transformed on to the interval $[-\frac{1}{2},\frac{1}{2}]$.

$$P_\nu(x) = \sum_{\mu<\nu+1}\alpha_\mu\,\tilde{T}_\mu(x), \quad P_\nu(\pm\tfrac{1}{2}) = 0, \tag{2.9a}$$

$$Q_\nu(x) = \sum_{\mu<\nu+2}\alpha_\mu\,\tilde{T}_\mu(x), \quad Q_\nu(\pm\tfrac{1}{2}) = \partial_x Q_{\nu|\pm\frac{1}{2}} = 0, \tag{2.9b}$$

The coefficients α_μ are chosen in such a way that the polynomials P_ν and Q_ν respectively form an orthogonal set and satisfy the boundary conditions given in (2.9). The beam-functions as well as the trigonometric functions can now be optionally replaced by the polynomials for one or more directions in the expansions of the velocity or the temperature. This offers the possibility of adapting the code to the given physical problem.

Applying the expansions (2.7), (2.8) in the Boussinesq equations (2.1) leads – together with the orthogonality condition – to a system of ordinary differential equations for the coefficients of the expansion. For the discretization of the time-derivatives, we employ an implicit method called the 'one-leg method', as described by Dahlquist (1976). This time-stepping method is of second-order accuracy and yields stable solutions even for large time-steps. More details of the numerical procedure are described in Kessler (1983, 1984).

As a result of the large domain of integration, three-dimensional, time-dependent numerical simulations require much CPU-time, even on modern vector computers. Therefore, we restrict our study to flow phenomena that are symmetric with respect

to the following conditions. First the mid-plane $y = 0$ is assumed to be a plane of symmetry, which means

$$\left.\begin{aligned} u(x,y,z) &= u(x,-y,z),\\ v(x,y,z) &= -v(x,-y,z),\\ w(x,y,z) &= w(x,-y,z),\\ \theta(x,y,z) &= \theta(x,-y,z). \end{aligned}\right\} \tag{2.10}$$

This symmetry implies that the coefficients b_{ijk}, d_{ijk} with even j and a_{ijk}, c_{ijk} with odd j must vanish. In addition, we assume point symmetry or axial symmetry of the flow field in the (x,z)-plane. The point symmetry enables us to calculate solutions with an odd number of convection rolls, while axial symmetry corresponds to solutions with an even number of convection rolls. These symmetry conditions can be written as follows:

$$\left.\begin{aligned} u(x,y,z) &= -u(-x,y,-z),\\ v(x,y,z) &= v(-x,y,-z),\\ w(x,y,z) &= -w(-x,y,-z),\\ \theta(x,y,z) &= -\theta(-x,y,-z), \end{aligned}\right\} \tag{2.11}$$

$$\left.\begin{aligned} u(x,y,z) &= -u(-x,y,z),\\ v(x,y,z) &= v(-x,y,z),\\ w(x,y,z) &= w(-x,y,z),\\ \theta(x,y,z) &= \theta(-x,y,z). \end{aligned}\right\} \tag{2.12}$$

The point symmetry (2.11) is equivalent to all coefficients a_{ijk}, d_{ijk} with even $i+k$ and b_{ijk}, c_{ijk} with odd $i+k$ in the expansion (2.7) being equal to zero. The axisymmetric solution is characterized by the fact that all coefficients a_{ijk}, d_{ijk} with even i and b_{ijk}, c_{ijk} with odd i must vanish. The symmetry conditions imposed on the numerical scheme can also be seen in real steady flows, provided that the Rayleigh number is slowly increased in the experiments (Jäger 1982). Therefore the symmetry conditions prove to be valid at least for steady calculations. But as soon as a variation of the number of rolls is accompanied by a change in symmetry, this physical process cannot be simulated by our numerical method. Considering an odd number of convection rolls, the symmetry of the flow is preserved even beyond the onset of oscillations. For an even number of convection rolls, the oscillatory modes observed in experiments break the symmetry in the (x,z)-plane, as the central zone of upward or downward motion no longer remains at a fixed point. Hence, the symmetry condition restricts our studies to an odd-number roll configuration in a box; a wavenumber dependence of the oscillation cannot be examined by our simulation. The transition from periodic to aperiodic or chaotic solutions is strongly influenced by symmetry conditions imposed on the numerical method, as was pointed out by McLaughlin & Orszag (1982). Therefore, the transition to aperiodic flows cannot be reproduced correctly by our numerical simulations. Nevertheless, the numerical method described above seems to be an efficient model for studying instability phenomena in the regime of periodic or quasiperiodic time-dependent flows.

The code has been tested in several ways. First, for the purposes of a comparison problem announced by Jones (1979), we calculated two-dimensional, steady solutions for the convection flow of air in a square cavity up to Rayleigh numbers of 10^7. These high Rayleigh numbers cause very thin boundary layers for the temperature and the velocity. Therefore, we use the polynomials defined above for each direction, setting the truncation parameters L and M equal to 22 and 16 respectively. A detailed comparison of the solutions of various authors was made by De Vahl Davis & Jones

				Frick *et al.* (1983)	
Ra	$L = M$	N	*Nu*	$L = M = N$	*Nu*
$30 \cdot 10^3$	8	8	3.649	8	3.702
	12	10	3.632	10	3.637
	16	12	3.611	12	3.610
$50 \cdot 10^3$	8	8	4.137	8	—
	12	10	4.117	10	4.142
	16	12	4.092	12	4.093
$70 \cdot 10^3$	8	8	4.473		—
	12	10	4.462		—
	16	12	4.434		—

TABLE 1. Nusselt number of square convection at infinite Prandtl number.

(1983). According to their report, most quantities of the Galerkin solution deviate by less than 1 % at a Rayleigh number of 10^6 and less than 0.3 % for the lower Rayleigh numbers of from the most accurate finite-difference and finite-element solutions. The test also illustrates that the Galerkin method needs more than three times fewer unknowns than finite-difference or finite-element methods for solutions with comparable accuracy.

In order to check the accuracy of the time-discretization of the code, the time evolution of a three-dimensional small-amplitude perturbation has been computed for various timesteps Δt. The growth rate as computed from the time evolution of the perturbation has been compared with corresponding eigenvalue calculations performed by Kirchartz (1980). The comparison of the solutions shows a deviation of approximately 0.6 %. This result is achieved for timesteps Δt lower than 0.01 and confirms the timestepping method used.

In order to verify the three-dimensional code in the strongly nonlinear region also, and in order to obtain information about the resolution of the code, we need quantitative comparisons at high Rayleigh numbers. We are not aware of detailed quantitative solutions with high accuracy in closed boxes for such high Rayleigh numbers. Therefore, for comparison purposes, we refer to the three-dimensional results of Frick, Busse & Clever (1983), who assumed periodic boundary conditions in horizontal directions. The different boundary conditions in horizontal directions can easily be implemented by replacing the beam-functions in horizontal directions by trigonometric functions in the expansion (2.7). This can be performed merely by the exchange of two statements in the code. Assuming an infinite Prandtl number, the so-called 'square convection' is calculated for various Rayleigh numbers and degrees of resolution. As a characteristic quantity, the dimensionless vertical heat transfer rates described by the Nusselt number *Nu* of the solutions are summarized in table 1 in comparison with the results of Frick *et al.* (1983). The agreement of the results with the best respective approximation to three decimal places is an excellent verification of the present code. Furthermore, the results confirm the good resolution of the temperature boundary layers at high Rayleigh numbers using 12 functions in the z-direction. The test also shows the importance of good horizontal resolution for the convergence of the vertical heat transfer. Moreover, considering the convergence rates of the solutions, we estimate an error of less than 0.4 % for the solutions with the best approximation.

case	(a)	(b)	(c)	(d)	(e)
T_1	30	34	38	42	46
T_2	16	20	24	28	32
T_3	29	33	37	41	45
N	3.178	3.414	3.542	3.498	3.510

TABLE 2. Time-averaged Nusselt number for various truncation parameters T_1, T_2, T_3; $Ra = 60000$; $Pr = 0.71$.

To achieve a comparable accuracy in the case of confined flows with a minimum of numerical effort, the truncation of the expansions (2.7) and (2.8) has to be adapted to the physical problem. Therefore, various calculations were performed to study the convergence of the solutions. For this test, we chose a Rayleigh number of 60000, a Prandtl number of 0.71 and conducting sidewalls, which is the most critical case with respect to the numerical resolution. Due to the relatively small vertical heat transfer rate in a small container at this Rayleigh number, the application of polynomials is not required. To achieve a comparable accuracy of the expansions (2.7) and (2.8) it is necessary to define different procedures for the truncation of each expansion. So the representation of $\psi^{(2)}$ requires a particularly high resolution in the x-direction, while we have to pay attention to a sufficient resolution in the y-direction of the scalar functions $\psi^{(1)}$, $\psi^{(31)}$ and $\psi^{(32)}$. The temperature θ, which is influenced by both parts of the velocity field, requires a comparably good resolution in all three directions in space. Therefore, the number of coefficients in (2.8) is chosen to be much higher than the number of coefficients in one of the velocity expansions (2.7). The various convergence tests show that a comparable accuracy for each direction can be achieved by neglecting all coefficients a_{ijk}, b_{ijk}, c_{ijk} and d_{ijk} which apply to the following relations:

$$4i+j+4k > T_1 \quad \text{for } a_{ijk}, c_{ijk}, \tag{2.13a}$$

$$i+3j+6k > T_2 \quad \text{for } b_{ijk}, \tag{2.13b}$$

$$i+2j+6k > T_3 \quad \text{for } d_{ijk}. \tag{2.13c}$$

The truncation parameters T_1, T_2 and T_3 are chosen in such a way as to guarantee an equal accuracy for all variables. The result of five calculations assuming different values for the truncation parameters T_1, T_2 and T_3 is summarized in table 2. We chose the time-averaged Nusselt number as a characteristic quantity for the comparison of the different solutions. The convergence of this parameter depends on the vertical resolution as well as on a sufficient resolution in the horizontal directions. The comparison of the results shows that the low resolution employed in the calculations (*a*) and (*b*) yields inaccurate values of the Nusselt number. Moreover, these calculations cannot reproduce the correct time evolution of the flow. By improving the resolution (case (*c*)) we can calculate a Nusselt number which deviates by less than 1 % from the best solution (*e*). Comparing the solutions (*e*) and (*d*), the calculated Nusselt numbers agree well with each other. The time evolution of both solutions is qualitatively identical and the frequency of the oscillations agrees with only 0.6 % deviation. Therefore the approximation used in case (*d*) is sufficient for the given physical problem and is employed for all calculations reported below, with an estimated error of about 1 %. Further, the test calculations result in the surprising fact that the resolution in time is less important for a correct description of the time

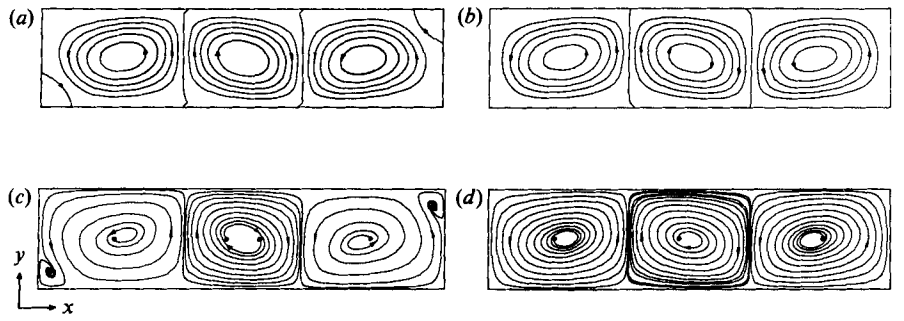

FIGURE 2. Streamlines of the steady convection for $Ra = 30000$ and $Pr = 0.71$, two-dimensional solution (*a*), (*b*), three-dimensional solution in the symmetry plane (*c*), (*d*), sidewalls are conducting (*a*), (*c*), or adiabatic (*b*), (*d*).

evolution of the solutions than the spatial resolution. In the following, we use about 40 timesteps for the calculation of one period of the oscillations at a Prandtl number of 0.71 and about 100 timesteps assuming a Prandtl number of 7.

3. Steady three-dimensional convection

The convection flow in a closed box is always three dimensional as a result of the no-slip condition at the vertical walls. The influence of this three-dimensionality strongly depends on the geometry considered. Nevertheless, it can be neglected for two special cases. The first one is the flow in a box with a large horizontal extent, which can be approximately described by means of analysis of infinite layers. The second case is the flow in a box with a very small horizontal extent in one direction, known as Hele-Shaw flow. In this flow, one component of the velocity tends to zero and a quasi-two-dimensional flow exists. However, considering containers with comparable horizontal and vertical dimensions, the influence of the sidewalls must be taken into account. This flow cannot be described satisfactorily by a two-dimensional model. The solutions obtained from two- or three-dimensional models shows principal differences especially in the regime of time-dependent flows. To study relations between the spatial structure and the dynamical behaviour of the flow, it is necessary to discuss first the three-dimensional effects in the steady flow. In the presence of rigid sidewalls there are two mechanisms leading to three-dimensional flow. The first one is the interaction of a rotating fluid with a stationary wall, where inertial forces induce an axial velocity within the rotating fluid. The second one, called thermal end effect, results from temperature gradients normal to the vertical walls. These gradients are caused by variations of the velocity field near the walls. As inertial forces in the flow field depend on the Prandtl number, the inertial end effect vanishes with an increasing value of this parameter. The thermal end effect, however, is determined by the thermal boundary condition of the sidewalls.

First of all we show some essential differences between the two- and three-dimensional convection flow by means of the streamline plots in figure 2. The steady two-dimensional convection with a Rayleigh number of 30000 and a Prandtl number of 0.71 is shown in the upper streamline plots of figure 2. The sidewalls are assumed to be conducting (figure 2*a*) or adiabatic (figure 2*b*). Contrary to the three-roll configuration calculated for adiabatic sidewalls, we can see two additional corner vortices in the case of conducting boundaries. Buoyancy forces induced by the

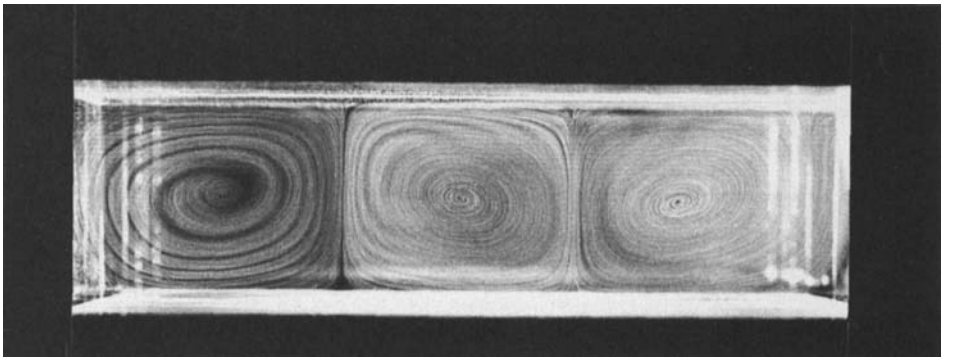

FIGURE 3. Light sheet photograph in the symmetry plane of the box at $Ra = 30000$, $Pr = 0.71$ and conducting sidewalls (Jäger 1982).

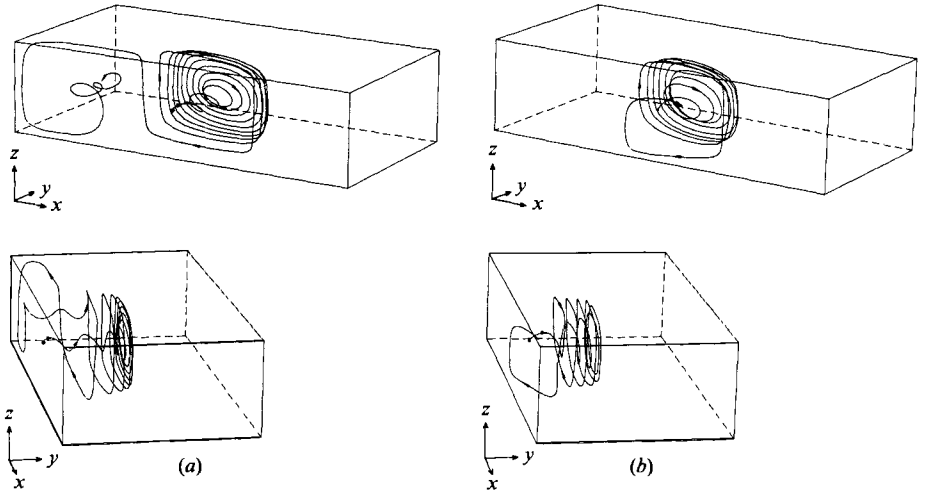

FIGURE 4. Streamlines of steady convection at $Ra = 30000$ and $Pr = 0.71$, adiabatic (a) and conducting (b) sidewalls.

temperature field near the wall are the reason for these vortices. These results can be compared with streamlines of the three-dimensional flow in the symmetry plane $y = 0$ (figure 2(c, d)), where the axial component of the velocity vanishes. The plots show that streamlines are no longer closed in the three-dimensional flow, but spiral out of the centres of the convection rolls. In contrast to the two-dimensional flow, an exchange of mass between the different rolls is observed. With conducting sidewalls, the streamlines beginning in the centres of the convection rolls all converge in the centres of the two corner vortices. However, with adiabatic boundaries, mass is transferred from the outer rolls to the central roll and the streamlines there converge into a limit cycle. The streamlines clearly show that the whole flow field is influenced by the vertical boundaries of the box. This is in good agreement with the experimental results of Jäger (1982) obtained for the same geometry. In figure 3 a light sheet photograph of the convection flow in air with a Prandtl number of 0.71 visualizes the particle traces in the symmetry plane. The boundary condition

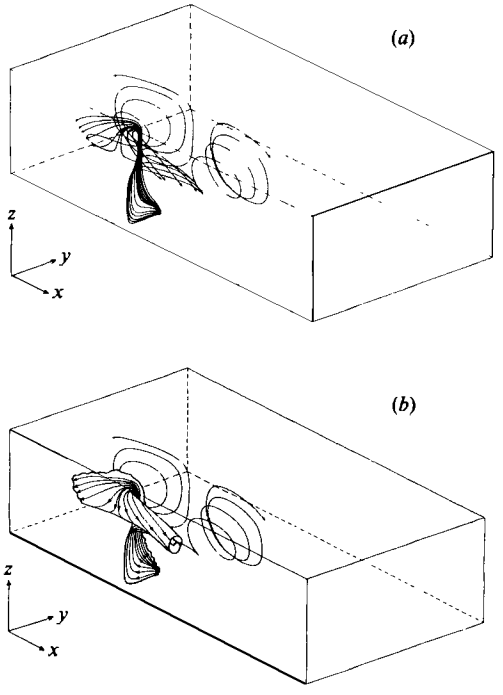

FIGURE 5. Streamlines (*a*) and principal sketch (*b*) of the secondary vortices at the front end of the convection rolls with conducting sidewalls.

of conducting sidewalls is well approximated by use of a glass frame for the vertical walls. The flow looks quite similar to the calculated streamlines of figure 2(*c*). The two corner vortices can be observed although partly hidden by light reflections from the sidewalls.

To give an impression of the general form of the three-dimensional flow some special streamlines are displayed in the following figures. For adiabatic sidewalls a streamline can be seen in figure 4(*a*) from different viewpoints. The streamline starts near the axis of the central convection roll and circulates helically toward the symmetry plane. After increasing its radius the streamline circulates back. Near the sidewall the streamline changes to the adjoining roll to start a similar motion. The principal behaviour of this three-dimensional flow, illustrated by this special streamline, confirms the inertial end effect described above. In figure 4(*b*) a streamline of the flow between conducting sidewalls is shown. In the central region of the box the streamline looks quite similar to that in figure 4(*a*). However, near the wall the flow is strongly three-dimensional, due to the temperature field in this region. The integration of some special streamlines starting near a critical point at the lower plate shows an interesting aspect of the flow near the wall (figure 5*a*). The singular streamsurface formed by these streamlines is sketched in figure 5(*b*) and visualizes secondary vortices at the front end of the convection rolls with an axis parallel to the x-direction.

As mentioned above, the influence of inertial forces depends on the value of the Prandtl number. With increasing Prandtl number inertial effects become less and less important. For moderate Rayleigh numbers the limit of an inertia-free motion is a good approximation for a Prandtl number of 7. In a convection flow of this higher Prandtl number the three-dimensionality only results from the thermal end-effect.

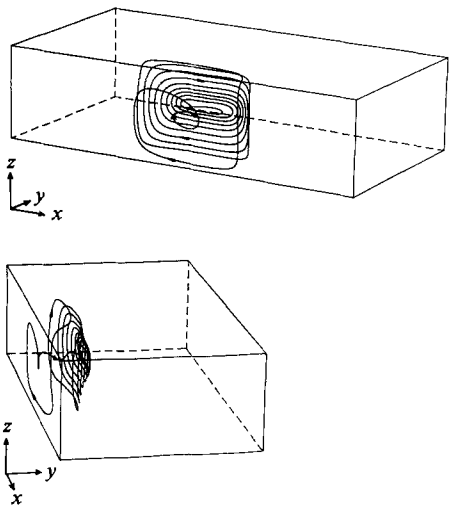

FIGURE 6. Streamlines of steady convection with $Ra = 30000$, $Pr = 7$ and adiabatic sidewalls.

The streamlines in figure 6 show that three-dimensional deformations of the flow are concentrated in regions near to the wall. The flow near the symmetry plane is approximately two-dimensional.

The solutions for steady convection flow show the strong influence of the thermal boundary condition on the three-dimensional structure of the flow. Changing the boundary condition from adiabatic to conducting causes two corner vortices and four longitudinal vortices at the front end of the convection rolls to appear. While the three-dimensionality caused by thermal effects is restricted to a small zone near the walls, the inertial end-effect causes a three-dimensional flow in the whole box. The consequences of these structural changes of the steady flow with respect to the dynamical behaviour will be discussed in the following section.

4. Time-dependent convection

With increasing Rayleigh number, the steady three-dimensional convection flow becomes unstable with respect to time-dependent disturbances. In general, the first time-dependent instability causes a periodic motion of the roll system. This is a three-dimensional process in which variations along the axis of the rolls, as well as the axial component of the velocity, play an important role. Therefore, the physical process of oscillations as it is observed in experiments cannot be reproduced by a two-dimensional model which neglects variations of the flow field in the axial direction. This is confirmed by two-dimensional, time-dependent calculations for Rayleigh numbers up to 400000 and a Prandtl number of 0.71. After a transient stage, which depends on the initial condition, all these time-dependent solutions converge to a steady state and no oscillation appears in this range of the Rayleigh number. An analogous result was found by Curry *et al.* (1984) for an infinitely extended fluid layer. They calculated a critical Rayleigh number for the onset of oscillations of about 39400 using a two-dimensional model, which is much higher than the corresponding value of 26200 obtained with the three-dimensional model. This clearly shows the importance of a three-dimensional simulation if we want to describe the dynamical behaviour of a flow correctly.

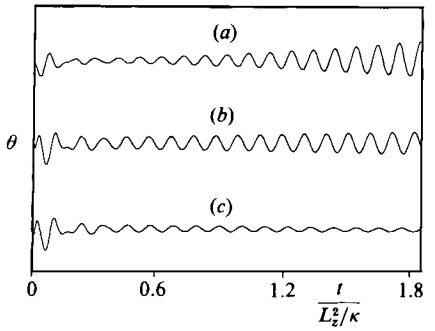

FIGURE 7. Time evolution of the temperature $\theta(-0.4L_z, 0, 0)$ at various Rayleigh numbers, $Pr = 0.71$ and conducting sidewalls. (*a*) $Ra = 36000$; (*b*) 34000; (*c*) 32000.

The critical Rayleigh number Ra_{osc} for the onset of the oscillatory instability is determined indirectly by nonlinear, time-dependent calculations. The time signal for the temperature at a fixed point in the symmetry plane is shown in figure 7 for a Prandtl number of 0.71 and three different Rayleigh numbers. The initial condition used causes a periodic time evolution which is amplified or damped depending on the Rayleigh number being above or below the critical value Ra_{osc}. By performing more calculations for various Rayleigh numbers, the critical Rayleigh number can be bounded and approximately determined. In this way, we obtain for a Prandtl number of 0.71 a critical value of 33200 ± 50 for conducting sidewalls and a slightly increased value of 33400 ± 50 assuming adiabatic sidewalls. With the present calculation, hysteresis effects at the bifurcation points cannot be detected. By increasing the Prandtl number to 7, the onset of oscillatory convection is shifted to a higher Rayleigh number of $Ra_{\mathrm{osc}} = 39000 \pm 100$. This Prandtl number dependence is qualitatively identical with the one observed in fluid layers of infinite extent. Our numerical results for the onset of oscillatory convection in air agree well with the critical value of 34000 experimentally determined by Jäger (1982). The geometry as well as the three-roll configuration and the boundary condition in his experimental set-up are the same as that assumed in our simulation. Gollub *et al.* (1980) measured a lower critical Rayleigh number of 29000 ± 1700 for the onset of oscillations in a slightly shorter box ($l_x = 3.5$, $l_y = 2.1$) and for a Prandtl number of 2.5. Experiments of Maurer & Libchaber (1980) for a similar geometry ($l_x = 3.5$, $l_y = 1.9$) filled with ^{4}He with a Prandtl number of 0.71, yielded a critical Rayleigh number of 23500, which is clearly lower than our calculated value. The reason for this discrepancy is found in the fact that they have a two-roll configuration in their box which is more unstable than a three-roll system.

Some information about the spatial structure of the oscillatory flow with a Prandtl number of 0.71 and conducting sidewalls is given by the series of plots shown in figure 8. Instantaneous streamlines and the corresponding isothermal lines in the symmetry plane $y = 0$ are shown for four different times, with the intervals being equal to one-quarter of a period. The piecewise streamlines are integrated up to a certain length to obtain a general impression of the flow structure in this plane without any information about the magnitude of the velocity. The streamline plots as well as the corresponding isotherms show a periodic motion of the locations of the upward and downward flow. This is accompanied by an alternating exchange of mass between the three convection rolls. In figure 8(*a*) fluid is transported from the outer rolls to

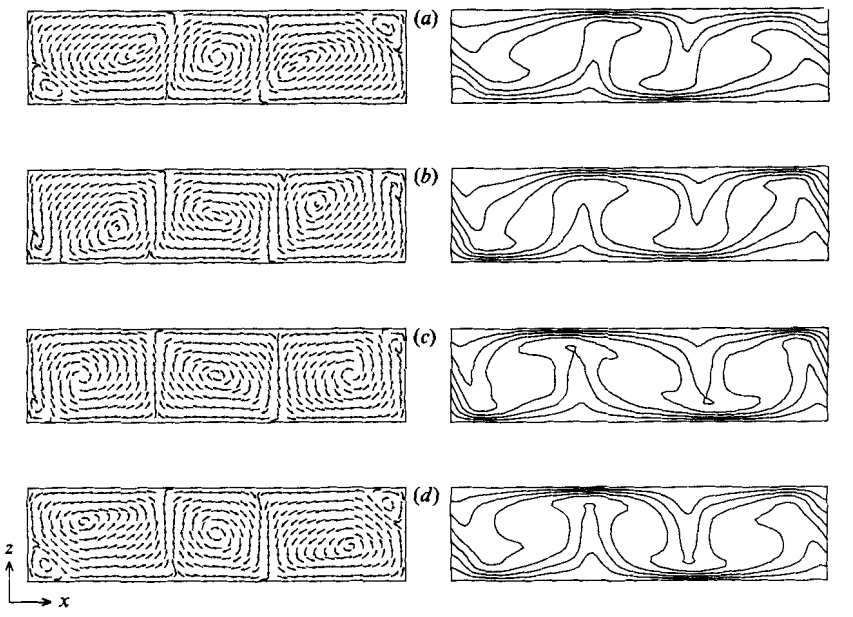

FIGURE 8. Instantaneous streamlines and isotherms in the symmetry plane $y = 0$ with $Ra = 38000$ and $Pr = 0.71$. (*a*) $t = 6.988$; (*b*) 7.012; (*c*) 7.036; (*d*) 7.060.

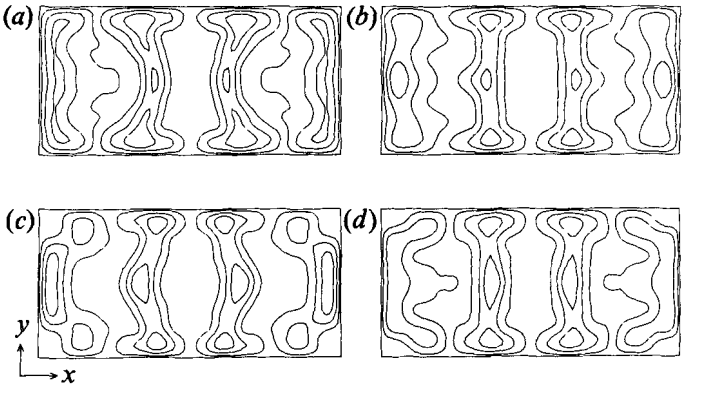

FIGURE 9. Isothermal lines in the plane $z = 0$ at $Ra = 38000$ and $Pr = 0.71$. (*a*) $t = 6.988$; (*b*) 7.012; (*c*) 7.036; (*d*) 7.060.

the small inner roll, which rotates faster than the outer ones. By increasing its horizontal extent, the inner roll decreases its rotational speed (figure 8*b*). In figure 8(*c*) the central roll has grown to its maximum size and a mass transfer begins from the centre roll to the two outer rolls. The inner roll now again decreases until the initial situation is achieved and one period of the oscillation is performed. To get more information about the three-dimensional oscillatory flow the temperature field in the ($z = 0$)-plane is displayed by a series of isothermal lines in figure 9. As the temperature in this plane is strongly coupled with the vertical component of the velocity, the extreme values of the temperature are nearly identical with the location of maximum downward and upward motions. The plots show that the oscillation has its maximum amplitude in the central region of the box and is very small near the vertical walls.

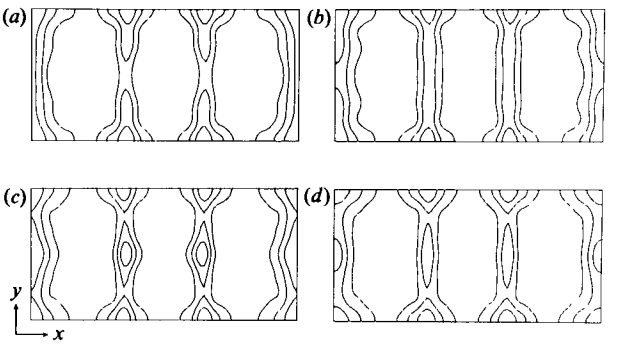

FIGURE 10. Isotherms in the plane $z = 0$ at $Ra = 50000$ and $Pr = 7$. (*a*) $t = 0.505$; (*b*) 0.515; (*c*) 0.525; (*d*) 0.535.

Therefore, the horizontal extent of the rolls strongly varies along the axial direction. This variation of the radius of the rotating fluid causes inertial forces which induce an axial velocity to the convection rolls. In the oscillating flow the direction of the axial velocity is changed periodically and fluid is transported from regions where the extent of the convection roll is large to regions where it is smaller. Together with alternating exchange of mass between the different rolls, this is the mechanism which maintains the oscillations of the flow with a Prandtl number of 0.71.

For an oscillatory solution of the flow in a box with adiabatic sidewalls, the results for the onset of the instability, as well as the frequency of the oscillation, differ only slightly from the data obtained for conducting walls. Although the three-dimensional structure of the flow strongly depends on the thermal boundary conditions, the physical process of the oscillations is not influenced by the thermal conditions at the walls. This can easily be understood by realizing the fact that oscillations mainly appear in the central regions of the box and that the three-dimensional flow near the walls is of secondary importance. The results presented above are in good agreement with recent numerical solutions obtained by Upson *et al.* (1983). Although the geometry and the Prandtl number assumed in their simulation differ slightly from the parameters we used, the main frequency agrees within 2 % deviation.

With increasing Prandtl number the inertial forces decrease and the behaviour of the oscillating flow changes dramatically. The series of plots showing isotherms in the $(z = 0)$-plane makes this obvious (figure 10). The Prandtl number of this simulation is 7 and the sidewalls are assumed adiabatic. The upward and downward motions occur at nearly fixed locations, while the maximum amplitude of the flow varies periodically along the axial direction. By comparing the results obtained for different Prandtl numbers, the importance of inertial forces with respect to the structure of oscillatory convection can be seen. While the oscillatory convection in a high Prandtl number flow is caused by thermal instabilities, the oscillating flow in a low-Prandtl-number fluid is a consequence of inertial forces in the flow.

A number of experiments in boxes show that a periodic flow is the first step in a sequence of instabilities. By increasing the Rayleigh number we want to examine which of the further instabilities can be found by the numerical simulation. To characterize the dynamical evolution of the calculated flow field we use power spectra analysis of the temperature θ at a fixed point $(-0.4L_z, 0, 0)$ of the symmetry plane. Figure 11 shows two sequences of power spectra obtained by simulating the convection flow in air for various Rayleigh numbers assuming either conducting (left)

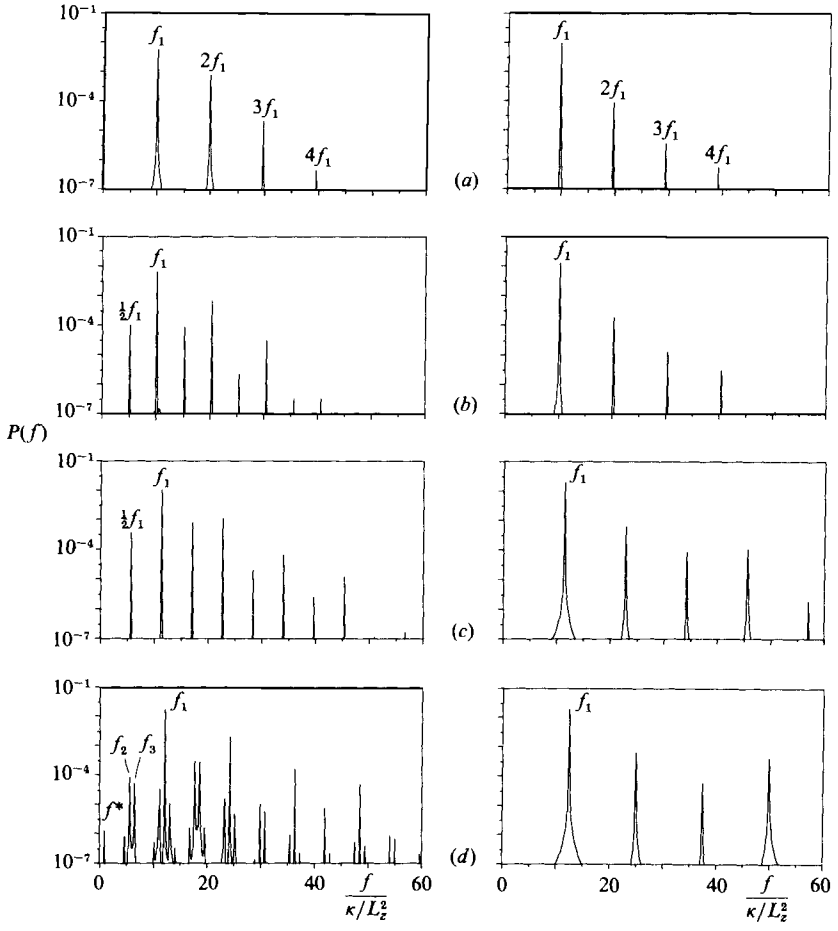

FIGURE 11. Sequences of power spectra of the temperature $\theta(-0.4L_z, 0, 0)$ assuming conducting (left) or adiabatic (right) sidewalls, $Pr = 0.71$. (*a*) $Ra = 38000$; (*b*) 40000; (*c*) 50000; (*d*) 60000.

or adiabatic sidewalls (right). Long-time simulations, including 30 periods or more, serve as the basis for the power spectra with an elimination of the transient effects in the time evolution. Considering the flow with a Rayleigh number of 38000 the spectra show a single main frequency and its higher harmonics, which means a periodic flow for both thermal boundary conditions. In a box with adiabatic sidewalls this periodic flow remains stable up to a Rayleigh number of 60000. The power spectra show solely an increasing main frequency and a varying amplitude of the higher harmonics when the Rayleigh number increases. A further instability does not occur in this range of the Rayleigh number. However, assuming conducting sidewalls we observe quite a different behaviour of the periodic flow. At a Rayleigh number of 40000 a subharmonic frequency and its combinations with the main frequency show up in the power spectrum. The amplitude of the subharmonic is about 10% of the amplitude of the main frequency. This oscillatory state is stable up to a Rayleigh number of about 56000 with slight variations of the amplitude ratio of the different frequencies. The onset of the subharmonic frequency might be explainable by a secondary time-dependent instability of the oscillating flow. The critical Rayleigh number for this instability is slightly beyond a value of 38000, and a small hysteresis

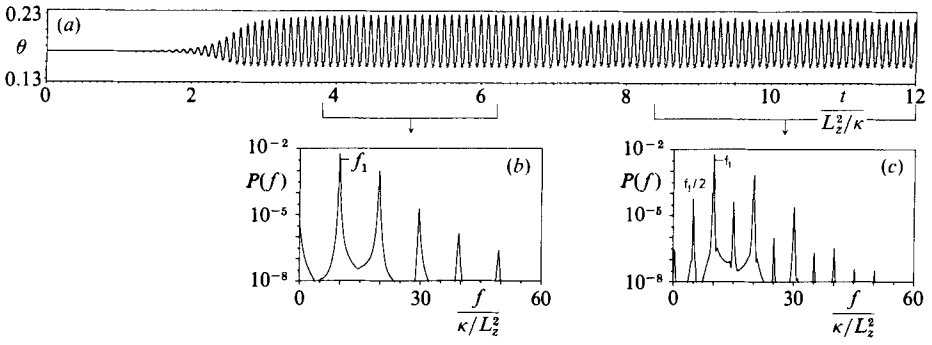

FIGURE 12. Time evolution of the temperature $\theta(-0.4L_z, 0, 0)$ at $Ra = 39000$, $Pr = 0.71$ and conducting sidewalls (*a*) and the corresponding power spectra before (*b*) and after the occurrence of the subharmonic frequency (*c*).

effect can be observed. The Rayleigh numbers of the two bifurcation points determined by increasing or decreasing the Rayleigh number respectively, only differ by a value of about 800. A long simulation at the Rayleigh number of 39000 gives an idea of this instability. The time evolution of the temperature is shown in figure 12 for this simulation. We start the calculation with a solution of the steady Boussinesq equation obtained for this Rayleigh number. This solution is unstable with respect to time-dependent disturbances and the round-off errors are sufficient to amplify the oscillatory instability. The amplitude of the oscillations first grows exponentially and then converges to a constant value. This oscillatory flow is preserved over more than 20 periods. A power spectrum of the temperature in this time interval shows a single frequency f_1 and its higher harmonics as observed for lower Rayleigh numbers. The further evolution in time shows a superposition of a disturbance of twice the period on to the oscillating temperature signal and a new stable flow is established. The corresponding power spectra now show the subharmonic frequency $\frac{1}{2}f_1$. As the Rayleigh number in this calculation is only slightly beyond the critical value for the onset of the subharmonic instability, the characteristic time for the growth of the amplitude is very long. Therefore, we observe many nearly undisturbed periods of the primary oscillation until the amplitude of the subharmonic disturbance has grown enough to influence the time evolution. However, at higher Rayleigh numbers the growth rate is increased and the secondary subharmonic instability can be seen immediately after the primary oscillation has reached its maximum amplitude.

At a Rayleigh number of 60000 a further bifurcation occurs and the periodic state is replaced by a quasi-periodic flow. The subharmonic peak splits into two frequencies f_2, f_3 with the small difference f^*. Many linear combinations of these frequencies indicate the strongly nonlinear character of this process. Note that none of the two frequencies f_2, f_3 is a subharmonic of the main frequency f_1. The two peaks are arranged symmetrically around the frequency $\frac{1}{2}f_1$, that is, the arithmetically averaged frequency of f_2 and f_3 is exactly $\frac{1}{2}f_1$. The physical meaning of such a spectrum can easily be seen in the corresponding time evolution of the temperature in figure 13. The subharmonic oscillation still appears, but with an amplitude modulated by the low frequency f^*.

The results presented above concerning the onset of a subharmonic instability clearly indicate the strong influence of the thermal boundary condition. At first sight

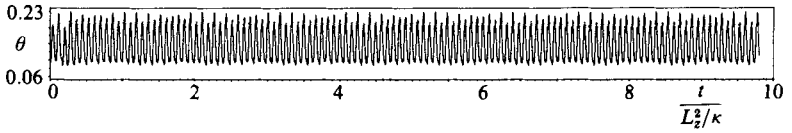

FIGURE 13. Time evolution of the temperature $\theta(-0.4L_z, 0, 0)$ at $Ra = 60000$, $Pr = 0.71$ and conducting sidewalls. The amplitude of the subharmonic is modulated with the frequency f^*.

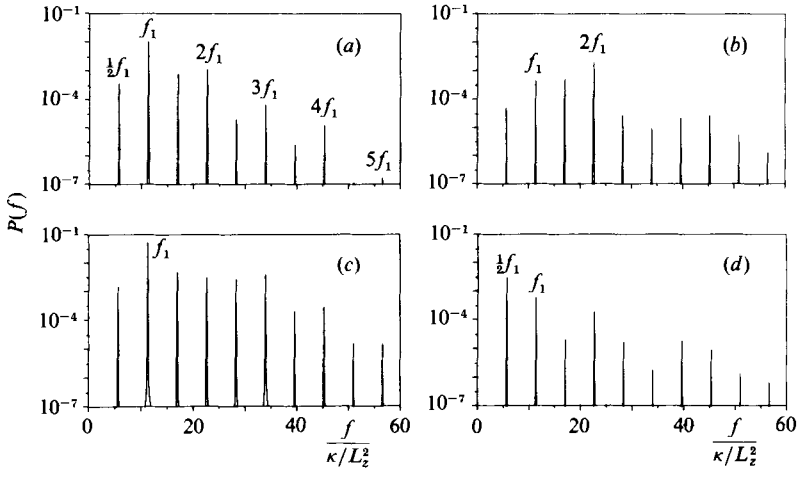

FIGURE 14. Power spectra of velocity and temperature at various locations for $Ra = 50000$ and $Pr = 0.71$. (*a*) temperature $\theta(-0.4L_z, 0, 0)$; (*b*) temperature $\theta(-0.55L_z, 0, 0)$; (*c*) velocity component $u(-0.55L_z, 0, 0)$ (*d*) temperature $\theta(-1.5L_z, 0.6L_z, -0.40L_z)$.

this is a surprising fact, since the primary oscillations of the flow are mainly restricted to the central region of the box, and no significant influence of the thermal boundary condition on this primary time-dependent instability is found. To clarify this strange behaviour of the flow we need more information about the spatial structure of the time-dependent flow field. The numerical simulation has the advantage that a solution, once it has been calculated and stored, can be analysed from various points of view. For example, there is the possibility of calculating power spectra of all variables at an arbitrary point in the flow field. A selection of the numerous spectra calculated is shown in figure 14 for a Rayleigh number of 50000, a Prandtl number of 0.71 and conducting sidewalls. A comparison of different power spectra shows that a frequency observed at an arbitrary point can be detected in the spectra of all variables in the whole flow field, provided that the resolution of the spectral analysis is sufficient. However, the amplitude of a certain frequency strongly depends on the location of the measurement and on the variable considered. This is illustrated by the four power spectra displayed in figure 14, all based on the same time interval of one solution. In figure 14 (*a*) a spectrum of the temperature at the point $(-0.4L_z, 0, 0)$ is shown. The main frequency f_1 dominates and the amplitudes of its higher harmonics decrease exponentially. By recording the power spectrum closer to the region of upwards motion, the amplitude of the first harmonic exceeds the main frequency f_1 (figure 14*b*), a known phenomenon which occurs near a periodically moving maximum of the variable considered. At the same location the power spectrum of the u-component of the velocity shows a maximum peak with the frequency f_1 (figure

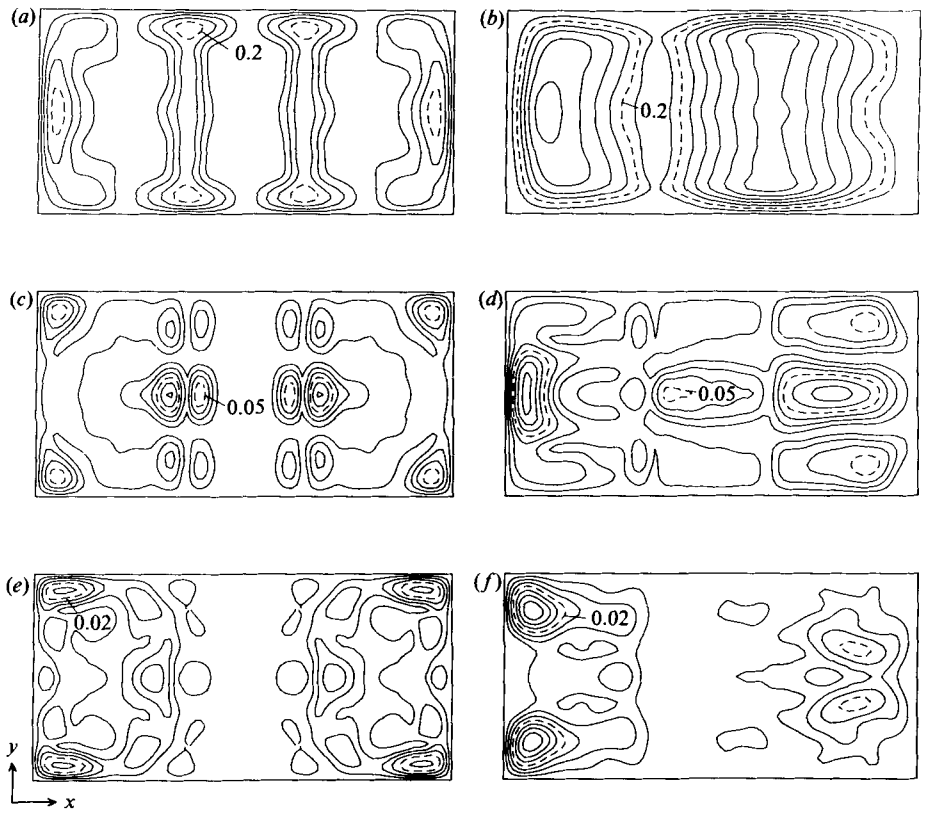

FIGURE 15. Contour plots of the temperature for the mean flow (*a*), (*b*), the amplitude of the oscillations f_1 (*c*), (*d*) and the amplitude of the subharmonic frequency $\frac{1}{2}f_1$ (*e*), (*f*) in the horizontal planes $z = 0$ (left) and $z = -0.35L_z$ (right).

14*c*). The ratio between the subharmonic peak and the main frequency also strongly depends on the location of the measurement. The subharmonic peak even dominates in a region near the corner of the box, as shown in the power spectrum of figure 14(*d*). The examples demonstrate the difficulties in characterizing a three-dimensional flow field by one single power spectrum recorded at one fixed point. The ratio of the different peaks in a power spectrum is not representative for the global flow field but depends on the spatial location. This must be taken into account, especially when comparing the time history of flows with different spatial structures. Therefore, without further information, the amplitude ratios of the peaks in a single power spectrum cannot imply the existence of a subharmonic frequency.

To clarify the influence of the thermal boundary conditions on the occurrence of bifurcations it is necessary to study the amplitude distribution of the different frequencies. Therefore, we decompose the flow variables at every point in the box into three different parts: a time-averaged value, an oscillating part with frequency f_1 and a subharmonic part with frequency $\frac{1}{2}f_1$. Further peaks are neglected in this decomposition. This way we not only get the time-averaged flow but also the spatial distribution of the oscillation and the subharmonic frequency $\frac{1}{2}f_1$. The oscillatory flow at a Rayleigh number of 50000 and a Prandtl number of 0.71 between conducting sidewalls is chosen for the decomposition. The results are plotted in figure 15 for the

horizontal planes $z = 0$ and $z = -0.35L_z$. The time-averaged temperature distributions are displayed in the two contour plots at the top of the figure. In the plane $z = 0$ (figure 15*a*) the regions of upward and downward motion of the convection flow can be clearly seen. The amplitude of the temperature oscillations with the frequency f_1 is illustrated by the contour maps of figure 15(*c*) and (*d*). In the midplane of the box we can recognize two maxima of the oscillation amplitude located in the central region of the box. This amplitude distribution is caused by the periodic motion of regions of upward and downward flow shown in figure 9. Further regions of large temperature fluctuations occur near the four corners. In the $(z = -0.35L_z)$-plane the maximum amplitude is shifted to the region near the left wall of the box. The amplitude distribution of the subharmonic frequency $\frac{1}{2}f_1$ differs from that of the primary oscillation (figure 15*e*,*f*). In the region of maximum amplitude of the oscillation f_1 the subharmonic frequency has only small amplitudes. In the midplane $z = 0$ the subharmonic is concentrated near the four corners. The maximum amplitude of the frequency $\frac{1}{2}f_1$, however, occurs near the left corners in the $(z = -0.35L_z)$-plane (figure 15*f*). At this location the amplitude of the subharmonic temperature fluctuations exceeds the amplitude of the primary oscillation. By comparing the regions of large subharmonic amplitudes with the topological structure of the three-dimensional flow, we obtain the interesting result that these regions correspond to the corner vortices caused by the conducting sidewall. This clearly shows a relation between the spatial structure of the flow and its evolution in time. The subharmonic bifurcation seems to be caused by the special three-dimensional flow field of the two corner vortices. In the absence of these corner vortices, in other words for adiabatic sidewalls, a subharmonic frequency cannot be detected in the whole range of Rayleigh numbers considered in these simulations.

5. Discussion

The numerical simulation of the convection flow in a box yields some interesting relations between the three-dimensionality of the flow and its dynamical evolution in time-dependent processes. For the case of rigid sidewalls the thermal end-effect and the inertial end-effect influence the flow in the whole region. The complex helical structure of the convection rolls caused by the inertial end-effect strongly depends on the Prandtl number and can be neglected for large-Prandtl-number fluids. By changing the thermal boundary conditions of the sidewalls from adiabatic to conducting boundaries, thermal effects increase and an additional system of secondary vortices is generated near the sidewalls. The numerical simulation proves to be a good tool for studying these three-dimensional effects. Integrated streamlines in connection with topological considerations give a good impression of the three-dimensional structure of the flow. Quantitative measurements of velocity components in a single plane, however, often give the impression of a nearly two-dimensional behaviour of the flow in the central region of the box. Details of the flow like the exchange of mass between neighbouring rolls, the helical structure of the rolls and the secondary vortices cannot be detected this way.

The critical Rayleigh number for the onset of oscillatory convection is determined approximately by nonlinear, time-dependent calculations. The onset of the oscillatory instability as well as its frequency are nearly independent of the choice of the thermal boundary conditions and the corresponding change in the flow structure. At low Prandtl numbers the oscillating flow is characterized by periodic displacements of the regions of upward and downward motion caused by inertial forces in the flow.

With increasing Prandtl number this instability is replaced by another oscillatory mode which is caused by a thermal instability only. A quantitative representation of these time-dependent instabilities can be obtained only by three-dimensional simulations.

In contrast to the oscillatory instability, the further bifurcations strongly depend on the spatial structure of the flow. For adiabatic sidewalls no further instability can be observed in the range of Rayleigh numbers considered. However, assuming conducting sidewalls, a subharmonic frequency can be observed with increasing Rayleigh number. The calculated threshold for the subharmonic agrees well with experimental data obtained by Gollub & Benson (1980), who find the first subharmonic bifurcation at a Rayleigh number of 36700 ± 800. Nevertheless, we have to keep in mind that some of the experimental parameters differ somewhat from the assumptions in our simulation. A relationship between this instability and the secondary corner vortices is shown by analysing the spatial structure of the time-dependent flow. The physical process leading to a subharmonic instability, however, cannot be identified clearly by this correlation. A hypothetical mechanism for this instability is discussed in the following. The primary oscillatory instability mainly occurs in the central region of the box. The flow near the sidewalls including the corner vortices is not involved in this instability. This fact is proved by comparing oscillating solutions obtained with different boundary conditions. However, the corner vortices are strongly coupled with the convection rolls via the varying mass exchange. So they can be considered as a secondary system which is forced by the oscillating convection rolls. Beyond the onset of the oscillatory instability the secondary system at first responds with oscillations of the frequency f_1. This is confirmed by maxima of the amplitude distribution of the primary oscillation at the corner vortices. Increasing the Rayleigh number causes a subharmonic response to appear in addition to the basic frequency, which is documented by the high amplitude of the frequency $\frac{1}{2}f_1$ in the region of the corner vortices. This phenomenon can be explained by a subharmonic resonance between the two oscillating systems. Further theoretical and experimental studies are necessary to clarify this physical process and to prove or to reject the explanation given above.

At higher Rayleigh numbers a splitting of the subharmonic peak is observed. The resulting two peaks are arranged symmetrically around the frequency $\frac{1}{2}f_1$ and differ by the low frequency f^*. So we obtain a quasi-periodic flow with a modulation in time of the subharmonic part of the oscillation. A rather similar effect was found in experiments of Gollub *et al.* (1980). For special initial conditions they observed a quasi-periodic motion which resulted also from a slow modulation in time of the second subharmonic of the oscillating flow. This comparison confirms that the quasi-periodic regime obtained by the numerical simulation is a real physical effect in the flow.

With a further increase of the Rayleigh number we obtain aperiodic solutions for both conducting and adiabatic sidewalls. We attribute this result to the insufficient spatial resolution of the numerical discretization at these high Rayleigh numbers. This is confirmed by the fact that the beginning of the aperiodic regime strongly depends on the number of basis functions used in the numerical method.

The numerical results presented above clearly show the importance of the spatial structure of the flow in order to explain the time evolution of this dynamical system. Secondary effects, like the appearance of the corner vortices, can change the dynamical behaviour of the flow fundamentally. Gollub *et al.* (1980) and McLaughlin & Orszag (1982) arrived at similar conclusions. The spatial structure of the primary

oscillation differs strongly from that of the subharmonic ones. So it seems unlikely that a simple model can yield quantitative predictions for such a flow without a reasonable consideration of the whole spatial structure of the system.

I would like to express my thanks to Professor H. Oertel, who initiated this work, for his encouragement and helpful discussions throughout this work. I would also like to thank Dr U. Dallmann and Dr E. Meiburg for valuable advice and for reviewing the manuscript. The work was partly supported by the Deutsche Forschungsgemeinschaft.

REFERENCES

BENJAMIN, T. B. 1978 Bifurcation phenomena in steady flows of a viscous fluid. 1. Theory. *Proc. R. Soc. Lond.* A **359**, 1–26.

BUSSE, F. 1981 Transition to turbulence in Rayleigh–Bénard convection. In *Hydrodynamic Instabilities and the Transition to Turbulence* (ed. H. L. Swinney & J. P. Gollub), pp. 97–137. Springer.

CURRY, J. H., HERRING, J. R., LONCARIC, J. & ORSZAG, S. A. 1984 Order and disorder in two- and three-dimensional Bénard convection. *J. Fluid Mech.* **147**, 1–38.

DAHLQUIST, G. 1976 Error analysis for a class of methods for stiff non-linear initial value problems. Lecture Notes in Mathematics, vol. 506 (ed. A. Dold & B. Echmann). Springer.

DAVIES-JONES, R. P. 1970 Thermal convection in an infinite channel with no-slip sidewalls. *J. Fluid Mech.* **44**, 695–704.

DAVIS, S. H. 1967 Convection in a box: linear theory. *J. Fluid Mech.* **30**, 465–478.

DE VAHL DAVIS, G. & JONES, I. P. 1983 Natural convection in a square cavity: a comparison exercise. *Intl J. Numer. Method. Fluid.* **3**, 227–248.

FEIGENBAUM, M. J. 1979 The onset spectrum of turbulence. *Phys. Lett.* A **74**, 375–378.

FRICK, H., BUSSE, F. H. & CLEVER, R. M. 1983 Steady three-dimensional convection at high Prandtl numbers. *J. Fluid Mech.* **127**, 141–153.

FRICK, H. & CLEVER, R. M. 1980 Einfluß der Seitenwände auf das Einsetzen der Konvektion in einer horizontalen Flüssigkeitsschicht. *Z. angew. Math. Phys.* **31**, 502–513.

GOLLUB, J. P. & BENSON, S. V. 1980 Many routes to turbulent convection. *J. Fluid Mech.* **100**, 449–470.

GOLLUB, J. P., BENSON, S. V. & STEINMAN, J. 1980 A subharmonic route to turbulent convection. *Ann. N.Y. Acad. Sci.* **357**, 22–27.

HARRIS, D. L. & REID, W. H. 1958 On orthogonal functions which satisfy four boundary conditions. *Astrophys. J.S.* **3**, 429–453.

JÄGER, W. 1982 Oszillatorische und turbulente Konvektion. Dissertation, Universität Karlsruhe, West Germany.

JONES, I. P. 1979 Natural convection in an enclosed cavity: a comparison problem. *Comp. Fluids* **7**, 315–316.

KESSLER, R. 1983 Oszillatorische Konvektion. Dissertation, Universität Karlsruhe, West Germany (DFVLR-Rep. FB-84-14).

KESSLER, R. 1984 Vectorization of the Galerkin method. In *Vectorization of Computer Programs with Applications to Computational Fluid Dynamics* (ed. W. Gentzsch), pp. 217–234. Vieweg.

KIRCHARTZ, K.-R. 1980 Zeitabhängige Zellularkonvektion in horizontalen und geneigten Behältern. Dissertation, Universität Karlsruhe, West Germany.

KOSCHMIEDER, E. L. 1981 Experimental aspects of hydrodynamic instabilities. In *Order and Fluctuations in Equilibrium and Non-Equilibrium Statistical Mechanics* (ed. E. Nicolis, G. Dewel & J. W. Turner), pp. 159–188. Wiley.

LIBCHABER, A. & MAURER, J. 1980 Une expérience de Rayleigh–Bénard de géométrie reduite: multiplication, accrochage et démultiplication de fréquences. *J. Phys. Paris* 41, 51–56.

LIBCHABER, A., LAROCHE, C. & FAUVE, S. 1982 Period doubling in mercury, a quantitative measurement. *J. Phys. Lett. Paris* **43**, L211–L216.

MCLAUGHLIN, J. B. & ORSZAG, S. A. 1982 Transition from periodic to chaotic thermal convection. *J. Fluid Mech.* **122**, 123–142.

MALLINSON, G. D. & DE VAHL DAVIS, G. 1977 Three-dimensional natural convection in a box: a numerical study. *J. Fluid Mech.* **83**, 1–31.

MAURER, J. & LIBCHABER, A. 1979 Rayleigh–Bénard experiment in liquid helium; frequency locking and the onset of turbulence. *J. Phys. Lett. Paris* **40**, L419–L423.

MAURER, J. & LIBCHABER, A. 1980 Effect of the Prandtl number on the onset of turbulence in liquid ^{4}He. *J. Phys. Lett. Paris* **41**, L515–L518.

OERTEL, H. 1980 Three-dimensional convection within rectangular boxes. In *Natural Convection in Enclosures* (ed. I. Catton & K. E. Torrance), pp. 11–16. ASME HTD, vol. 8.

STORK, K. & MÜLLER, U. 1972 Convection in boxes: experiments. *J. Fluid Mech.* **54**, 559–611.

UPSON, C. D., GRESHO, P. M., SANI, R. L., CHAN, S. T. & LEE, R. L. 1983 A thermal convection simulation in three dimensions by a modified finite element method. In *Numerical Properties and Methodologies in Heat Transfer* (ed. T. H. Shih), pp. 245–259. Hemisphere.

ZIEREP, J. & OERTEL JR, H. 1981 *Convective Transport and Instability Phenomena*. Braun.